Bioelectrochemistry 155 (2024) 108588

Contents lists available at ScienceDirect

Bioelectrochemistry

journal homepage: www.journals.elsevier.com/bioelectrochemistry

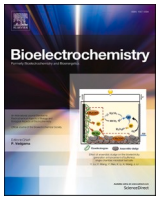

Cellular excitability and ns-pulsed electric fields: Potential involvement of lipid oxidation in the action potential activation

Lea Rems [a,*], Aurianne Rainot [b], Daniel Wiczew [b], Natalia Szulc [b], Mounir Tarek [b,*]

[a] University of Ljubljana, Faculty of Electrical Engineering, SI-1000 Ljubljana, Slovenia
[b] Université de Lorraine, CNRS, LPCT, F-54000 Nancy, France

ARTICLE INFO

Keywords:
Cell membrane
Electroporation
Lipid oxidation
Molecular dynamics simulations
Hodgkin-Huxley models
Voltage-gated ion channels

ABSTRACT

Recent studies showed that nanosecond pulsed electric fields (nsPEFs) can activate voltage-gated ion channels (VGICs) and trigger action potentials (APs) in excitable cells. Under physiological conditions, VGICs' activation takes place on time scales of the order 10–100 μs. These time scales are considerably longer than the applied pulse duration, thus activation of VGICs by nsPEFs remains puzzling and there is no clear consensus on the mechanisms involved. Here we propose that changes in local electrical properties of the cell membrane due to lipid oxidation might be implicated in AP activation. We first use MD simulations of model lipid bilayers with increasing concentration of primary and secondary lipid oxidation products and demonstrate that oxidation not only increases the bilayer conductance, but also the bilayer capacitance. Equipped with MD-based characterization of electrical properties of oxidized bilayers, we then resort to AP modelling at the cell level with Hodgkin-Huxley-type models. We confirm that a local change in membrane properties, particularly the increase in membrane conductance, due to formation of oxidized membrane lesions can be high enough to trigger an AP, even when no external stimulus is applied. However, excessive accumulation of oxidized lesions (or other conductive defects) can lead to altered cell excitability.

1. Introduction

Electrostimulation is an indispensable tool in treatment of various acute and chronic conditions, including cardiac pacing and defibrillation [1,2], treatment of drug-resistant migraines [3,4], Parkinson disease [5], epilepsy [6], bladder disorder [7], and many others. Stimulation of the target tissue is achieved by applying electrical pulses with duration that conventionally ranges from tens of microseconds to milliseconds. Recently, shorter pulses with duration from a few to hundreds of nanoseconds have been receiving increasing attention, as they can potentially offer important benefits, including stimulation at lower delivered energies reducing thermal damage [8] and the possibility to focus the electric field at considerable distance from the electrodes [9]. Such nanosecond pulsed electric fields (nsPEFs) have been shown to provoke electrical signals (action potentials) in various excitable cells, including cultured neurons [10,11], peripheral nerve fibers [12–14], cardiomyocytes [15,16], and neuroendocrine cells [17–19]. However, it remains unclear how pulses with such short durations are able to excite the cells.

Cellular excitability is mediated mainly by specific transmembrane proteins called voltage-gated ion channels (VGICs). VGICs sense changes in the local transmembrane voltage and respond by undergoing conformational rearrangements that close or open the channel, allowing selective conduction of ions (Na^+, K^+, Cl^- or Ca^{2+}) along their electrochemical gradient. The selective and sequential opening of different ion channels then leads to a characteristic change in the transmembrane voltage – the action potential (AP). The activation of VGICs (though by much weaker voltage changes) is known to take tens to hundreds of microseconds [20,21]. The shortest time for activating sodium voltage-gated (Na_V) channels, which are responsible for the initiation of an AP, was estimated to be 11 μs [13]. How can then nsPEFs, which are considerably shorter than this time, trigger APs?

nsPEFs are primarily known as a mean to permeabilize cell membranes [22]. This process termed electroporation results at least in part from conformational rearrangement of the lipids forming the cell membrane when subject to sufficiently intense electric fields, resulting in formation of aqueous pores within the lipid bilayer. Several groups have conducted studies to investigate the effects of nsPEFs specifically

* Corresponding authors at: University of Ljubljana, Faculty of Electrical Engineering, Tržaska 25, SI-1000 Ljubljana, Slovenia; CNRS, Unité Mixte de Recherches 7565, Université de Lorraine, Boulevard des Aiguillettes, BP 70239, 54506 Vandoeuvre-lès-Nancy, France.
E-mail addresses: lea.rems@fe.uni-lj.si (L. Rems), mounir.tarek@univ-lorraine.fr (M. Tarek).

https://doi.org/10.1016/j.bioelechem.2023.108588
Received 21 January 2023; Received in revised form 10 October 2023; Accepted 10 October 2023
Available online 12 October 2023

on excitable cells. In adrenal chromaffin cells, the effect of nsPEFs was found to depend on the duration of the pulse. Exposure of these cells to 5 ns, 50 kV/cm pulses triggered indeed a sodium (Na^+) influx that depolarized the membrane and activated multiple voltage-gated calcium (Ca_V) channels (L-, N- and P/Q-type channels) increasing the intracellular concentration of Ca^{2+} [17,18]. On the other hand, when exposed to a single nsPEF of longer duration (150 to 400 ns), Ca_V channels appeared to not be the only pathway for Ca^{2+} influx. In fact, their total inhibition led to only a 67 % reduction of Ca^{2+} uptake. Accordingly the authors concluded that the uptake was also due to Ca^{2+} influx through pores formed in the cell membrane by the electric field (electroporation) [19]. For peripheral nerves, stimulation by 12 ns pulses was shown to trigger APs and sustained tetanus, implying that nsPEFs can activate, through a still unknown mechanism, VGICs without electroporative injuries [12]. Using a fast-responding voltage-sensitive dye (FluoVolt), the same group showed that an AP can also be triggered in rat hippocampal neurons by a 200 ns pulse of sufficient amplitude. However, they found that the threshold electric field for AP initiation and electroporation are very similar, making it challenging to determine whether Na_V channels are directly activated by nsPEF or indirectly due to leak currents resulting from electroporation [11]. A recent molecular dynamics study suggested that nsPEFs can move charged residues responsible for Na_V activation; however, these residues move randomly and inconsistently, making direct activation of the channels by the applied electric field questionable [23].

Due to these confounding results (see [24] for a review), there is no clear consensus on the underlying mechanism taking place and leading to electrostimulation when cells are subject to nsPEFs. Pakhomov and Pakhomova [24] proposed three alternative mechanisms: (1) the applied electric field induces sufficiently long membrane depolarization that lasts well after the applied pulse, enough to activate VGICs (similarly as in conventional stimulation); (2) the applied electric field leads to electroporation and formation of pores in the cell membrane, which enable nonselective leak current and, as such, depolarize the membrane and activate VGICs; or (3) a combination of the two.

Here we propose yet another possible mechanism that has so far been

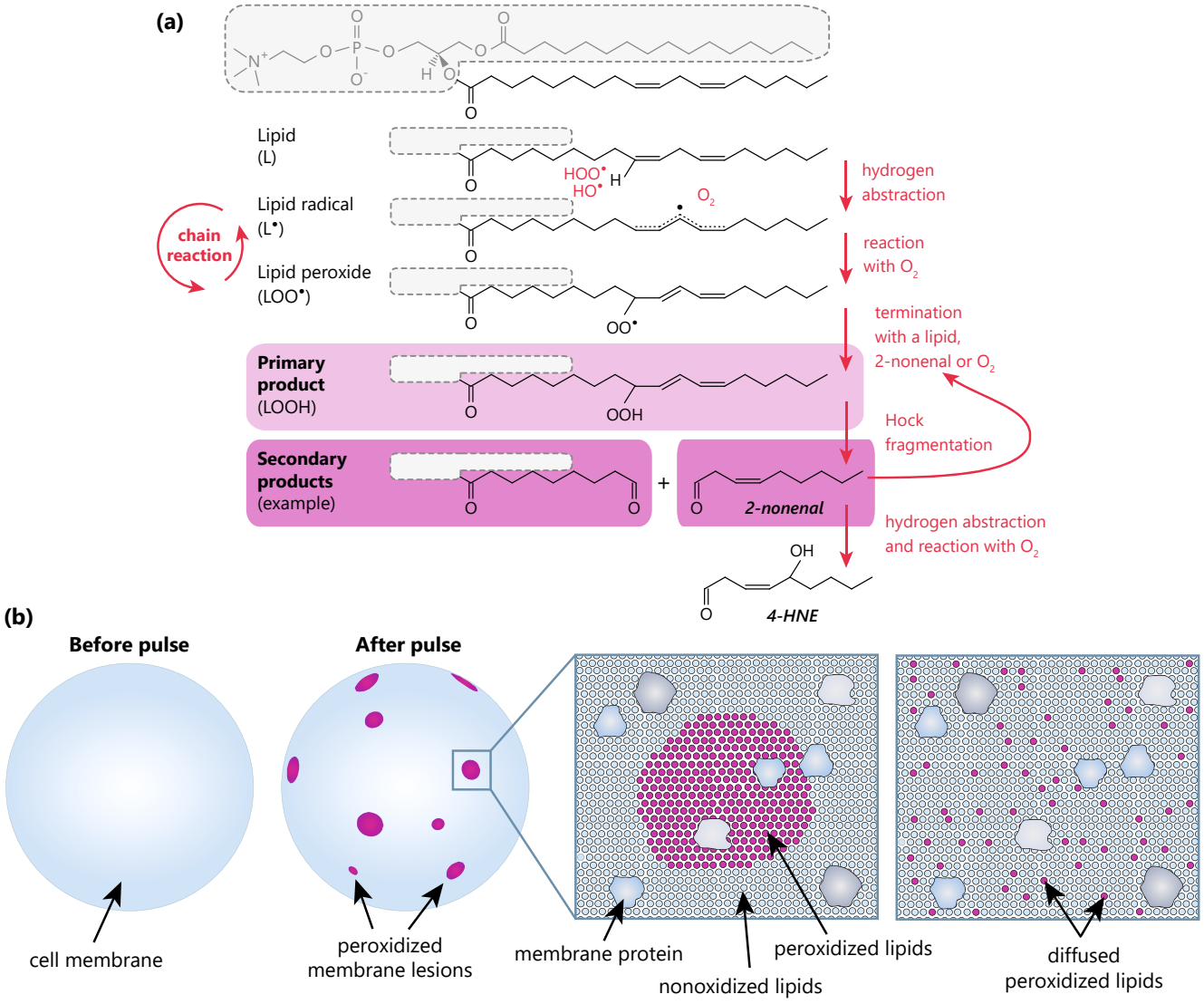

Scheme 1. Lipid oxidation. (a) Pathway for primary and secondary oxidation of a phospholipid (L) containing a single bis-allylic site, e.g., linoleic acid. The primary oxidation is a multistep process leading to the generation of lipid hydroperoxides LOOH. The intermediate formation of a lipid radical leads to hydrogen abstraction from an adjacent lipid, which initiates a chain reaction in which the radical damage is propagated along neighboring lipids, creating highly oxidized membrane lesions. The secondary oxidation can occur through Hock fragmentation with the formation of 2-nonenal. 2-nonenal can be a hydrogen donor for $LOO^•$ radical and transfer the radical to another lipid initiating yet another chain reaction [28,29,37]. (b) Schematic representation of oxidized membrane lesions, which are expected to form in the cell membrane after exposure to nsPEF. The schematic is hypothetical, and the lesions are not drawn to scale. The images on the right depict the molecular organization in one of the lesions, immediately after nsPEF and later in time as the oxidized lipids laterally diffuse. Figure inspired by [38,39].

overlooked. nsPEFs are known to generate both intra- and extra-cellular reactive oxygen species (ROS) [25,26], which can lead to oxidative damage of polyunsaturated lipids. This damage is initiated when a free radical, such as HO$^{\bullet}$ or HOO$^{\bullet}$, abstracts an allylic or bis-allylic hydrogen in the polyunsaturated lipid tail, leading to the formation of a lipid radical L$^{\bullet}$ (Scheme 1a). L$^{\bullet}$ reacts with molecular oxygen, which is highly abundant in the membrane's interior [27], to form a lipid peroxide radical LOO$^{\bullet}$. The latter may further abstract hydrogen from another lipid to form a hydroperoxide LOOH, i.e., the primary oxidation product. The lipid neighbor with abstracted hydrogen may further propagate the damage to adjacent lipid, initiating a chain reaction, the result of which is creation of highly oxidized lesions (patches) in the lipid membrane (Scheme 1b). Lipid hydroperoxides can then convert directly or indirectly into secondary products of oxidation – lipids with truncated tails ending with either an aldehyde or carboxylic group [28,29]. Importantly, creation of primary and secondary lipid oxidation products, induced by nsPEFs as well as longer pulses used traditionally for electroporation, has been confirmed in lipid vesicles and cultured cells [30–36].

The presence of oxidized lipids dramatically changes the membrane electrical properties. In our previous studies we showed that the membrane conductance increases by up to several orders of magnitude with increasing fraction of oxidized lipids [38,39]. However, as oxidation changes the membrane thickness and polarity [38,39], we expect that membrane capacitance changes upon oxidation as well. Both the change in membrane capacitance and conductance can provoke changes in the transmembrane voltage. Our aim here is to assess whether, and under which conditions, these changes can activate Na_V channels and trigger an AP. Thus, in this study we first use computational chemistry methods to characterize the capacitance of membranes with increasing percentage of primary or secondary lipid oxidation products. We then use mathematical modeling based on Hodgkin-Huxley description of APs to show how the changes in membrane capacitance and, even more importantly, membrane conductance caused by lipid oxidation are sufficient to trigger an AP.

2. Methods

2.1. Molecular dynamics (MD) simulations

2.1.1. System preparation

As depicted in Scheme 1b, lipid oxidation leads to the formation of membrane lesions (patches) with high content of oxidatively damaged lipids. Furthermore, oxidized lipids ultimately diffuse laterally, which progressively lowers their local concentration. Accordingly, we studied systems representing membrane patches with both high and low content of either primary or secondary lipid oxidation products.

To model membrane patches containing primary oxidation products we prepared lipid bilayers consisting of mixtures of 1,2-dilinoleoyl-*sn*-glycero-3-phosphocholine (DLPC) and one of its peroxidized forms (EE13, see Fig. 1a). We considered five different bilayer systems with increasing percentage of EE13 lipids: 0 %, 12.5 %, 25 %, 50 % to 100 %.

To model membrane patches containing secondary oxidation products we also prepared five different bilayer systems consisting of mixtures of 1-palmitoyl-2-oleoyl-*sn*-glycero-3-phosphocholine (POPC) and 1-palmitoyl-2-(9-oxononanoyl)-*sn*-glycero-3-phosphocholine (PoxnoPC, see Fig. 1b). The percentage of PoxnoPC was varied from 0 %, 5 %, 10 %, 20 % to 50 %.

All lipid bilayers (128 lipids per leaflet) were bathed in sodium chloride aqueous solutions. The exact composition of all systems is reported in Table 1. Note that the ionic concentration of the bath does not influence the value of the capacitance (results not shown).

2.1.2. Parameters

The CHARMM36 [40] force-field was used to describe the non-oxidized lipids, the ions, and the TIP3P water molecules. For EE13 and PoxnoPC, the force-fields used were developed by us, as previously described [39,41]. The molecular dynamics (MD) simulations were performed using Gromacs 2018 [42]. The leap-frog algorithm was used to integrate the equations of motion, with a time step of 2.0 fs. Particle Mesh Ewald (PME) [43,44] was used to calculate the long-range electrostatic interactions. A switching function was used between 1.0 nm and 1.2 nm to smoothly bring the van der Waals forces and energies to 0 at 1.2 nm. LINCS [45] was used to constrain the chemical bonds between hydrogens and the heavy atoms to their equilibrium values. 3D periodic boundary conditions were applied.

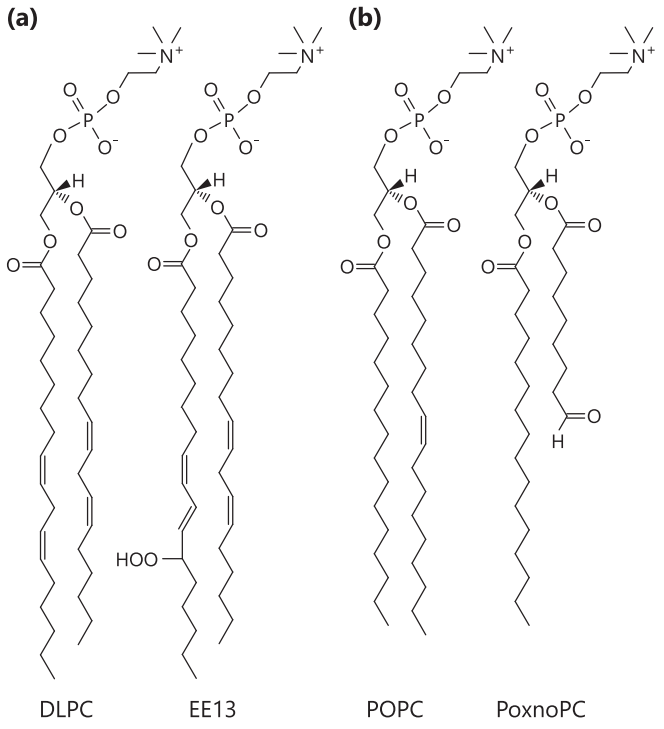

Fig. 1. Structure of the lipids considered in this study. (a) DLPC and its primary oxidation product EE13. (b) POPC and its secondary oxidation product PoxnoPC.

Table 1
Composition of the modeled systems: number of each lipid, number of water molecules, number of sodium and chloride ions, and the dimensions of the simulation box.

Primary products	DLPC	EE13	water	Na	Cl	Simulation box (nm^3)
100 % DLPC	256	0	17,444	96	96	9.0 × 8.9 × 16.0
12.5 % EE13	224	32	17,536	96	96	8.7 × 9.0 × 16.0
25 % EE13	192	64	17,612	96	96	9.2 × 9.0 × 16.0
50 % EE13	128	128	17,428	96	96	9.6 × 9.6 × 16.0
100 % EE13	0	256	22,976	96	96	10.0 × 10.0 × 16.0
Secondary products	**POPC**	**PoxnoPC**	**water**	**Na**	**Cl**	**Simulation box (nm^3)**
100 % POPC	256	0	22,012	28	28	9.0 × 9.0 × 20.0
5 % PoxnoPC	244	12	21,252	28	28	9.1 × 9.1 × 16.0
10 % PoxnoPC	230	26	22,138	28	28	9.2 × 9.2 × 16,0
20 % PoxnoPC	204	52	22,301	28	28	9.3 × 9.3 × 16.0
50 % PoxnoPC	128	128	22,712	28	28	9.5 × 9.5 × 16.0

2.1.3. Equilibration

The bilayers were first equilibrated in the *NPT* ensemble maintaining the pressure *P* at 1 bar (using the Parrinello-Rahman barostat [46]) and the temperature *T* at 303 K (using Nosé-Hoover thermostats [47,48]). The evolution of the area per lipid was monitored to confirm that the

systems were equilibrated during MD runs of 100 ns and 300 ns, respectively, for bilayers containing primary and secondary oxidation products.

2.1.4. Capacitance calculation

To estimate the capacitance of the model systems, we used the single bilayer setup previously introduced by Delemotte et al. [49,50]. Briefly, void slabs were created along the normal (z axis) to the membrane in order to separate the ionic baths from their periodic images. Such a setup allows for modeling adequately the system at a constant charge imbalance, if the latter is created at the initial configuration of the MD run (for instance by generating a difference between the overall charge of the two bilayer surroundings). In practice, starting from a system at no charge imbalance, we displaced one, two, …, monovalent ions of the same sign from one side of the bilayer to the other to create net charge imbalances Q of 0e, 2e, 4e, …, where e is the elementary charge. As the bilayer behaves as a capacitor (an insulator), the charge imbalance induces a difference in the electrostatic potentials between the two ionic baths, as shown in Fig. 2a. This transmembrane voltage U is related to the capacitance per unit area of the membrane (i.e., specific membrane capacitance C) and the imposed charge imbalance per unit area Q_s via:

$$C = Q_s/U \tag{1}$$

The electrostatic potential V along axis z can be derived from the MD trajectory using the 1D Poisson's equation as the double integral of the charge density $\rho(z)$:

$$V(z) - V(-L) = -\int_{-L}^{z} dz' \int_{-L}^{z'} \rho(z'')dz''/\varepsilon_0 \tag{2}$$

where ε_0 is the vacuum permittivity and L is half the box length in the z direction. For each system described in Table 1, MD simulations of 20 ns, carried out at constant volume and temperature ($T = 303$ K), were used to estimate the electrostatic potentials at $Q = 0e$, 2e, 4e, and 6e. Linear fits to the obtained transmembrane voltage U were used to retrieve the value of the capacitance, as shown in Fig. 2b.

2.2. Modeling action potential generation

All simulations were carried out using Comsol Multiphysics 6.0 (Comsol Inc., Burlington, MA, USA), as described below. All models are available at https://github.com/learems/Oxidation-Excitation.

2.2.1. Equivalent circuit model

The most widely used mathematical model of neuronal AP originates from Hodgkin and Huxley [51]. The membrane is represented as a capacitor and three resistors representing the ionic currents flowing through sodium, potassium and other (leak) channels (Fig. 3a). The resistors depend on the transmembrane voltage to account for the voltage-dependent opening and closing of the ion channels. The resistors' conductances (inverse of their resistances) are given by:

$$G_{Na} = g_{Na}m^3h \tag{3a}$$

$$G_K = g_K n^4 \tag{3b}$$

$$G_L = const. \tag{3c}$$

The gating functions m, n, and h have values between 0 and 1 and evolve according to differential equations:

$$\frac{dm}{dt} = \alpha_m(1-m) - \beta_m m \tag{4a}$$

$$\frac{dn}{dt} = \alpha_n(1-n) - \beta_n n \tag{4b}$$

$$\frac{dh}{dt} = \alpha_h(1-h) - \beta_h h \tag{4b}$$

where α_x and β_x ($x = m$, n, or h) depend on the transmembrane voltage and can be understood as transition rates between given states of the channels. α_x and β_x can have different mathematical forms, depending on which experiments they were fitted to; we here take equations from [52], which were fitted to measurements on pyramidal cortical neurons:

$$\alpha_n = 0.020\,\mathrm{ms}^{-1}\frac{u-25}{1-\exp\left(-\frac{u-25}{9}\right)} \tag{5a}$$

$$\alpha_m = 0.182\,\mathrm{ms}^{-1}\frac{u+35}{1-\exp\left(-\frac{u+35}{9}\right)} \tag{5b}$$

$$\alpha_h = 0.250\,\mathrm{ms}^{-1}\exp\left(-\frac{u+90}{12}\right) \tag{5c}$$

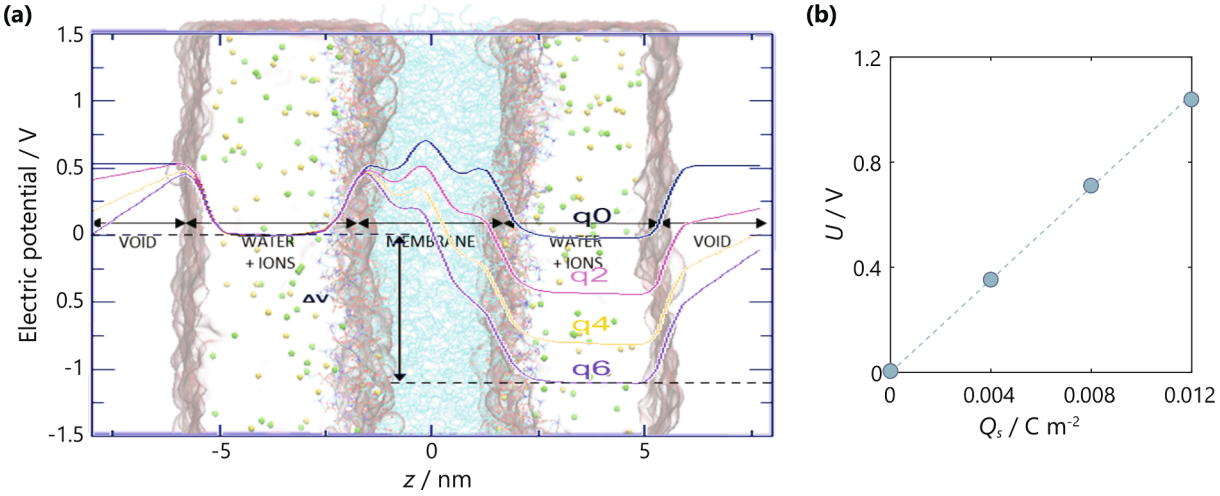

Fig. 2. Calculating bilayer capacitance with MD simulations. (a) Electrostatic potential along the z axis for the 100 % DLPC system. The transmembrane voltage U is the difference between electric potentials $V(z)$ in the two ionic baths. The center of the bilayer is at $z = 0$ nm. (b) The capacitance is retrieved by plotting U as a function of Q_s. Linear regression (dashed line) is used to retrieve the value of the capacitance.

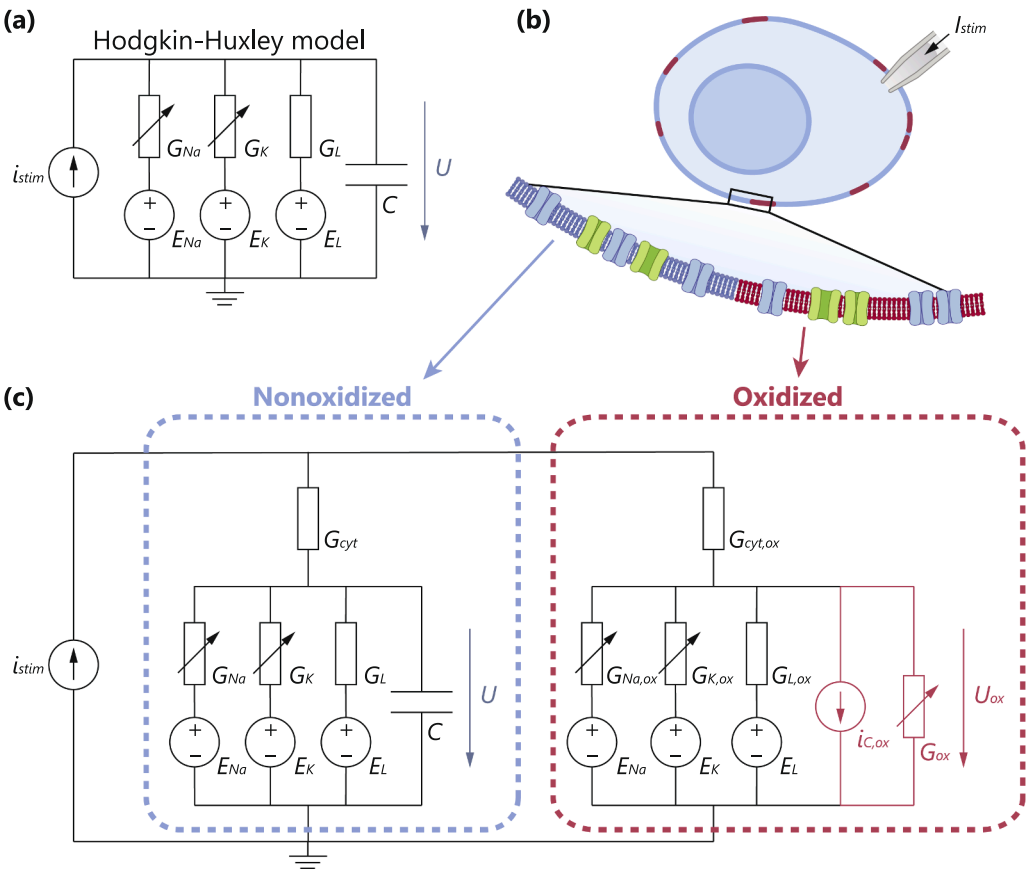

Fig. 3. The equivalent circuit model based on Hodgkin-Huxley description of a neuronal membrane. (a) Scheme of the original Hodgkin-Huxley equivalent electrical circuit. (b) Schematic representation of a non-oxidized and oxidized membrane patch, both containing VGICs. (c) Modified Hodgkin-Huxley equivalent circuit, considering two membrane patches depicted in (b). Note that the increase in membrane capacitance in the oxidized patch is modeled using a current source, described in eq. (6b).

$$\beta_n = -0.002\,\mathrm{ms}^{-1}\frac{u-25}{1-\exp\left(-\frac{u-25}{9}\right)} \tag{5d}$$

$$\beta_m = -0.124\,\mathrm{ms}^{-1}\frac{u+35}{1-\exp\left(-\frac{u+35}{9}\right)} \tag{5e}$$

$$\beta_h = 0.250\,\mathrm{ms}^{-1}\frac{\exp\left(\frac{u+62}{6}\right)}{\exp\left(\frac{u+90}{12}\right)} \tag{5f}$$

where u is a nondimensionalized transmembrane voltage

$$u = \frac{U}{1\,\mathrm{mV}} \tag{5 h}$$

and $U = V_i - V_e$ is defined as the difference between the electric potentials at the intracellular (V_i) and extracellular (V_e) side of the membrane.

To study the influence of lipid oxidation on the AP generation, we modified the original Hodgkin-Huxley circuit to represent two patches of a cell membrane, one with non-oxidized lipids and one that becomes oxidized upon nsPEF exposure, as depicted in Fig. 3b-c. To each of the patches we added a series resistor G_{cyt} representing the resistance of the intra- and extra-cellular fluid. The value of G_{cyt} was chosen such that the membrane charging time in either of the patches was 100 ns [53]. Whereas the non-oxidized patch resembled the original Hodgkin-Huxley circuit, the circuit representing the oxidized patch was modified to account for the change in membrane capacitance and conductance upon oxidation.

To correctly model the change in membrane capacitance in the oxidized patch, we considered the following. The electric current in a capacitor is defined as:

$$I_{C,ox} = \frac{dQ_{ox}}{dt} = \frac{d(C_{ox}U_{ox})}{dt} \tag{6a}$$

$$I_{C,ox} = C_{ox}\frac{dU_{ox}}{dt} + \frac{dC_{ox}}{dt}U_{ox} \tag{6b}$$

where Q_{ox}, U_{ox}, and C_{ox}, and are capacitor's charge, voltage, and capacitance, respectively. Typically, we consider that the capacitance is constant, simplifying (6b) to $I_{C,ox} = C_{ox}dU_{ox}/dt$. However, in our case dC_{ox}/dt is nonzero. To implement the full equation (6b) in Comsol, we modelled the capacitor as a current source with the current defined by (6b). The capacitance was defined with a time-dependent function

$$C_{ox}(t) = C_0 + C_0(f_{increase} - 1)h\left(t - t_{delay}, t_{ox}\right) \tag{7}$$

where C_0 is the initial membrane capacitance, $f_{increase}$ is the factor by which the membrane capacitance increases due to lipid oxidation, and $h(t - t_{delay}, t_{ox})$ is a switching function that changes from 0 to 1 within time t_{ox} at time t_{delay}. This switching function was implemented with Comsol's smoothed Heaviside function *flc1hs* that has a continuous first derivative:

$$h(t,t_{ox}) = flc1hs(t,t_{ox}) = \begin{cases} 0 & t \le -t_{ox} \\ 1 & t \ge t_{ox} \\ 0.5 + 0.75(t/t_{ox}) - 0.25(t/t_{ox})^3 & -t_{ox} \le t \le t_{ox} \end{cases} \quad (8)$$

The time derivative dC_{ox}/dt was computed with Comsol's built-in differentiation operator $d(C_{ox}, t)$.

To include also a change in membrane conductance due to lipid oxidation, we added to the oxidized patch circuit an additional resistor, which conductance changed with the time-dependent function

$$G_{ox}(t) = G_{ox}h\left(t - t_{delay}, t_{ox}\right) \quad (9)$$

The values of model parameters are reported in Suppl. Table S1. Since the kinetics of lipid oxidation, promoted by exposure to nsPEF, is not clear, we arbitrarily set $t_{ox} = 1$ μs, considering that oxidation is a fast process and is expected to occur during or immediately after exposure to nsPEF. Nevertheless, our results are not very sensitive to the choice of t_{ox}; as shown in the Suppl. Table S2, we tested different values of t_{ox} (between 10 ns and 10 ms) and found no difference in the minimum oxidized areas required to trigger an AP. This minimum area began to slightly increase when $t_{ox} = 100$ ms. According to [11], membrane depolarization upon nsPEF occurs within < 1 ms.

The equivalent circuit and the differential equations (4a-c) were implemented in Comsol using the *Electrical Circuit* interface and the *Global ODEs and DAEs* interfaces, respectively. The system of equations was solved with direct solver MUMPS, using a fully coupled approach and a *strict* time stepping method. An initial 100-ms-long equilibration simulation was performed in the absence of any stimulus or changes in membrane properties, to bring all variables to their initial steady state. The result from this simulation was used as the initial condition for all other simulations.

2.2.2. Whole-cell model

To model APs at the cell level, we considered a spherical cell placed in an extracellular domain, either in 2D axisymmetric geometry (Fig. 4a) or 3D geometry (Fig. 4b), following previous studies [54–56]. The electric potential distribution V in the intracellular and extracellular domain was determined by

$$\nabla \bullet \left[\left(\sigma_{i,e} + \varepsilon_{i,e} \frac{\partial}{\partial t} \right) \nabla V_{i,e} \right] = 0 \quad (10)$$

where $\sigma_{i,e}$ and $\varepsilon_{i,e}$ denote, respectively, the conductivity and the dielectric permittivity of the intracellular (subscript *i*) or extracellular (subscript *e*) medium. Two opposite sides of the extracellular domain were modeled as electrodes by assigning them an electric potential. When simulating the response to an external electric field, the positive electrode (anode) was excited by a rectangular pulse of chosen duration and amplitude, while the negative electrode (cathode) was kept at 0 V.

The cell membrane was modeled via a boundary condition, which describes the continuity of the normal component of the electric current density $\mathbf{J_e}$ across the membrane

$$\mathbf{n} \bullet \mathbf{J}_e = G_{tot}U + C_{tot}\frac{\partial U}{\partial t} + \frac{\partial C_{tot}}{\partial t}U + J_{channels}$$

$$J_{channels} = G_{Na}(U - E_{Na}) + G_K(U - E_K) + G_L(U - E_L) \quad (11)$$

where $\mathbf{n}$ denotes the unit vector normal to the membrane surface. Transmembrane voltage $U = V_i - V_e$ is the difference between the electric potentials on the two sides of the membrane. G_{tot} and C_{tot} denote the membrane conductance and membrane capacitance, respectively. $J_{channels}$ describes the electric current through ion channels, where G_{Na}, G_K, and G_L are defined by equations (3–5).

To model changes in membrane properties caused by lipid oxidation, G_{tot} and C_{tot} were considered a function of time and space. G_{tot} and C_{tot} were made to change from their baseline to a given value at a chosen time t_{delay} with the Comsol function *flc1hs* having a risetime of t_{ox} (see also Section 2.2.1 and equations (7–9)). In addition, G_{tot} and C_{tot} changed only in distinct circular regions (oxidized lesions) on the cell membrane. In the 2D axisymmetric model, a single region was defined around one of the poles of the cell (Fig. 4a). This region was defined by an angle that corresponds to a spherical cap of a chosen area (chosen areal fraction of the cell membrane):

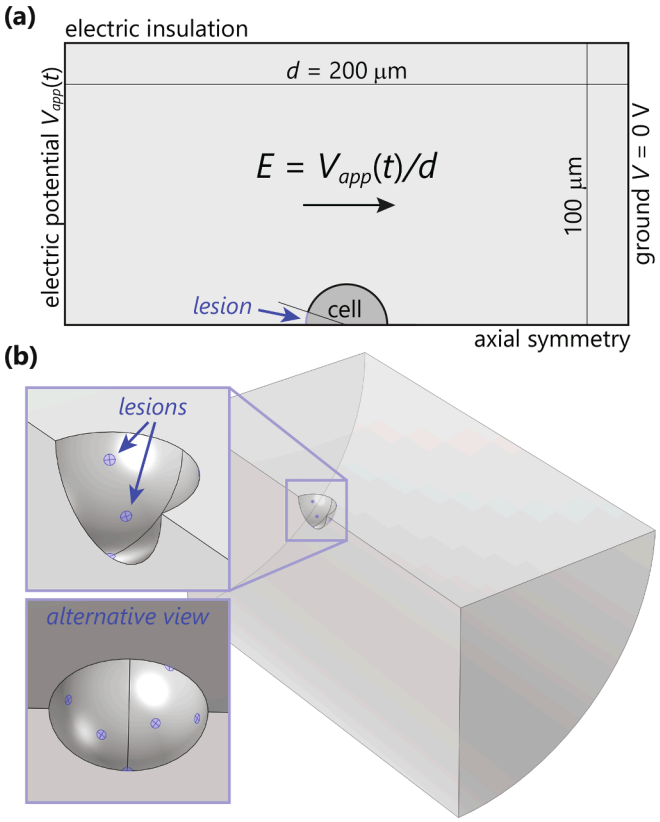

Fig. 4. Geometry of the whole-cell models. (a) 2D axisymmetric model of a spherical cell in an extracellular medium. (b) Corresponding 3D model. Due to symmetry only a quarter of the cell was modelled.

$$\theta_{ox} = \text{acos}\left(1 - \frac{A_{ox}}{2\pi {R_{cell}}^2}\right) \quad (12)$$

In the 3D model, we considered that there are 20 oxidized lesions of a chosen area distributed randomly along the membrane (Fig. 4b). Due to symmetry, and to facilitate computation, we represented only a quarter of the entire geometry in the simulations. When simulating the response to the change in G_{tot} and C_{tot}, no electric field was applied, and the two sides representing the electrodes were both kept at 0 V.

In both the 2D axisymmetric and 3D model, equation (10) was implemented with two *Electric Currents* interfaces, one for the extracellular and one for the intracellular domain. Equation (11) was implemented within *Electric Currents* interface with a *Normal Current Density* boundary condition. Equations (4a-c) were implemented each with a separate *Boundary ODEs and DAEs* interface. The mesh around the lesions was refined by limiting the maximum element size (10 nm in proximity of the lesion(s), 300 nm elsewhere along the membrane). The system of equations was solved with direct solver MUMPS, using a fully coupled approach and a *strict* time stepping method. An initial 100-ms-long equilibration simulation was performed in the absence of any stimulus or changes in membrane properties, to bring all variables to their initial steady state. The result from this simulation was used as the initial condition for all other simulations. The values of all model parameters are reported in Suppl. Table S3.

3. Results

3.1. Membrane capacitance locally increases due to oxidative lipid damage

We first used MD simulations to model two systems consisting of patches of oxidized lipids, representative of lesions caused by either primary or secondary oxidation of respectively DLPC and POPC. The integrity of the bilayer DLPC-EE13 was conserved for all considered percentage of the primary oxidation product, lipid hydroperoxide EE13, while the bilayer POPC-PoxnoPC lost its integrity (i.e. pores were formed) when the percentage of secondary oxidation product PoxnoPC reached ≥ 80 %, as previously reported [39]. By quantifying the specific membrane capacitance (in $\mu F/cm^2$) of all modeled systems, we observed that the capacitance increases substantially as the percentage of oxidized lipid increases (Fig. 5a). This is expected, as oxidation increases the number of polar entities in the membrane (water, peroxide or aldehyde group). The factor by which the capacitance increases with respect to non-oxidized value is more profound when the bilayers contain secondary oxidation products (Fig. 5b).

3.2. Increase in membrane capacitance can trigger an AP: The electrostatic approximation

Each VGIC possesses a specific threshold of activation and deactivation, i.e., transmembrane voltage at which the channel undergoes conformational rearrangements that open or close its inner ion conduction pathway. When the membrane depolarizes from its resting voltage to a certain threshold (around −55 mV for neuronal membrane), an AP initiates mainly thanks to the opening of Na_V channels (Fig. 6a). The influx of Na^+ then further depolarizes the membrane. Around +40 mV Na_V channels inactivate, and voltage-gated potassium (K_V) channels activate causing an efflux of K^+, repolarizing the membrane back to the resting voltage. Hence, in cell's excitability, the threshold voltage plays a key role in the initiation of the AP.

In the following we investigate, if the increase in membrane capacitance due to lipid oxidation could depolarize the membrane enough to initiate an AP. A cell membrane acts as capacitor (thin insulator) that separates intra and extra-cellular media. The ionic distributions within these two media, maintained by ion channels and pumps, give rise to an ionic or "charge" imbalance Q_s and a specific resting transmembrane voltage U_r. U_r can hence be expressed as

$$U_r = Q_s/C_0 \tag{13}$$

where C_0 is the baseline membrane capacitance.

When an oxidized lesion is formed, the membrane capacitance locally increases. Considering equation (13) and assuming at first approximation that Q_s in cells is maintained constant by ionic pumps and channels, a change in the local capacitance from C_0 to C would induce a change of the local transmembrane voltage from U_r to U, that can be determined as:

$$U = U_r C_0/C = U_r/f_{increase}$$

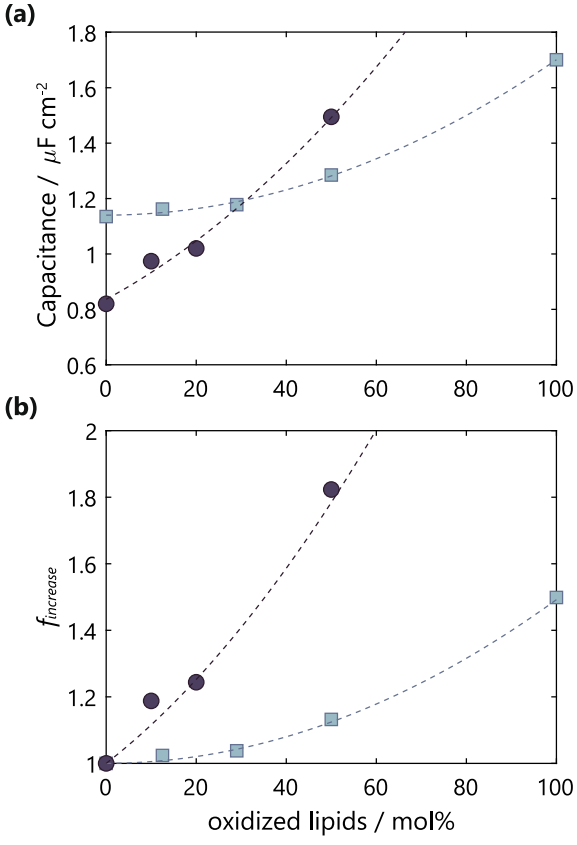

Fig. 5. Capacitance of bilayers containing oxidized lipids, determined with MD simulations. Capacitance was determined for DLPC-EE13 lipid bilayers with 0 %, 12.5 %, 25 %, 50 % and 100 % of primary lipid oxidation product EE13 (■) and POPC-PoxnoPC lipid bilayer with 0 %, 5 %, 10 %, 20 % and 50 % of secondary lipid oxidation product PoxnoPC (●). Capacitance is expressed in (a) absolute values and (b) as a factor of increase with respect to nonoxidized value, $f_{increase} = C/C_0$. Dashed lines show best fit with a quadratic polynomial function.

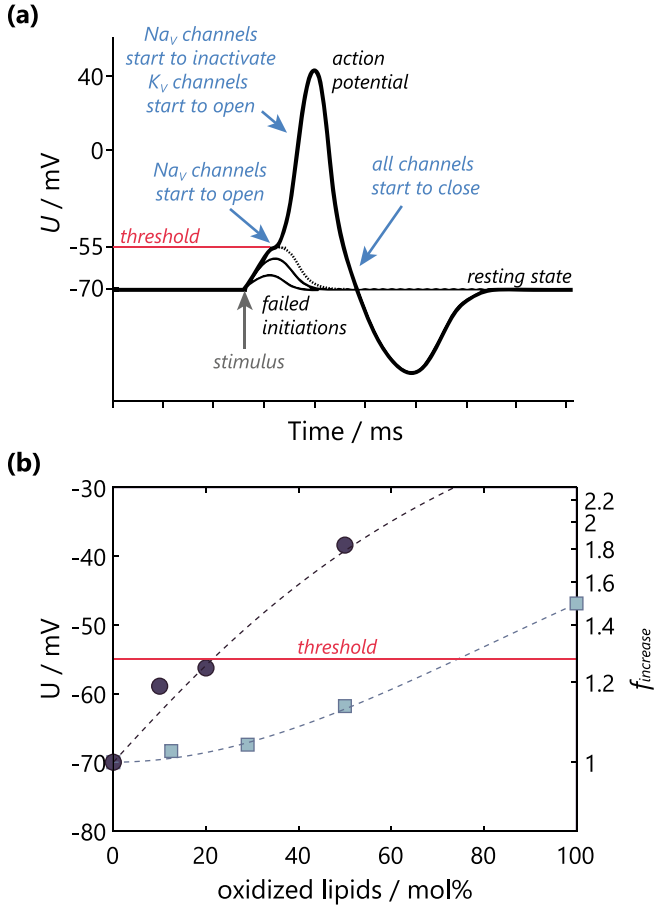

Fig. 6. Change in membrane capacitance could potentially trigger an AP. (a) Shape of a typical AP. (b) Local membrane depolarization caused by an increase in membrane capacitance due to the presence of primary (EE13, ■) or secondary (PoxnoPC, ●) lipid oxidation products.

$$f_{increase} = C/C_0 \quad (14)$$

Fig. 6b shows the calculated U using capacitance values from Fig. 5 and considering a typical resting voltage of the neuronal membrane $U_r = -70$ mV. When the local capacitance increases, the local transmembrane voltage becomes less negative, i.e., the membrane depolarizes. If this depolarization is enough to reach the threshold for activation of Na_V channels, that reside within the oxidized lesion, we hypothesize that an AP could be triggered. Indeed, the estimates shown in Fig. 6b suggest that in membrane lesions containing more than ~70 % or ~20 % of primary or secondary oxidation products, respectively, the increase in membrane capacitance is sufficient to reach the threshold required to activate Na_V channels.

3.3. Increase in membrane capacitance can trigger an AP: The equivalent circuit model

We next consider a Hodgkin-Huxley-type equivalent circuit to describe the full temporal dynamics of AP generation. The equivalent circuit (Fig. 3c) presents two parts of a neuronal membrane with Na_V, K_V, and other (leak) channels. One part of the membrane is considered to remain non-oxidized, whereas the second is considered to become oxidized upon nsPEF exposure.

Let us first study the response of the equivalent circuit to stimulation by a conventional 1 ms-long electric current pulse applied at $t = 10$ ms, the entire membrane remaining non-oxidized (no change in membrane electrical properties). Fig. 8a shows that sufficiently large positive (inward) currents depolarize the membrane and open Na_V channels, which triggers an AP. On the contrary, negative (outward) currents hyperpolarize the membrane without triggering an AP.

Now let us examine the response to a change in membrane capacitance occurring suddenly at $t = 10$ ms as a results of lipid oxidation. Herein, no electric stimulus is applied, only the capacitance in the second membrane part is increased by a given factor. For simplicity, we consider that the area of the oxidized part of the membrane is equal to the area of the non-oxidized part. Fig. 7 b shows that under such circumstances, an increase in membrane capacitance by a factor of 1.2 or more triggers an AP, corroborating the estimates presented in Section 3.2.

Representation of both the non-oxidized and oxidized parts of the membrane in the equivalent circuit allows us to explore further the membrane areal fraction that needs to be oxidized in order to trigger an AP. We set the total membrane area arbitrarily to 1000 μm (roughly the area of a typical cell of radius ~10 μm), and then we vary the fraction of the oxidized lesions from 0 % to 95 %. Fig. 8 shows the minimum areal fraction of oxidized lesions able to trigger an AP, depending on the factor of increase in membrane capacitance. An increase by factor of 1.5–1.8, corresponding to the maximum capacitance change upon oxidation determined with MD (Fig. 5b), requires at a minimum 10 % of the membrane area oxidized. This is not unreasonable, since mammalian cells often contain in their plasma membrane more than 50 % of polyunsaturated lipids [57], which are highly susceptible to oxidative lipid damage.

3.4. Increase in membrane conductance is even more important compared to the increase in membrane capacitance

For completeness one should however recall that lipid oxidation is not only associated with an increase in membrane capacitance, but also an increase in membrane conductance, as demonstrated in our previous studies [38,39]. The values of the latter, reported in Table 2, indicate for instance that the conductance of a membrane lesion containing 100 % EE13 lipid hydroperoxides is 26 S/m^2, whereas a lesion containing 50 % PoxnoPC has a conductance of 2000 S/m^2.

To model an increase in membrane conductance, we added an additional resistor to the equivalent circuit, as shown in Fig. 3c, and we

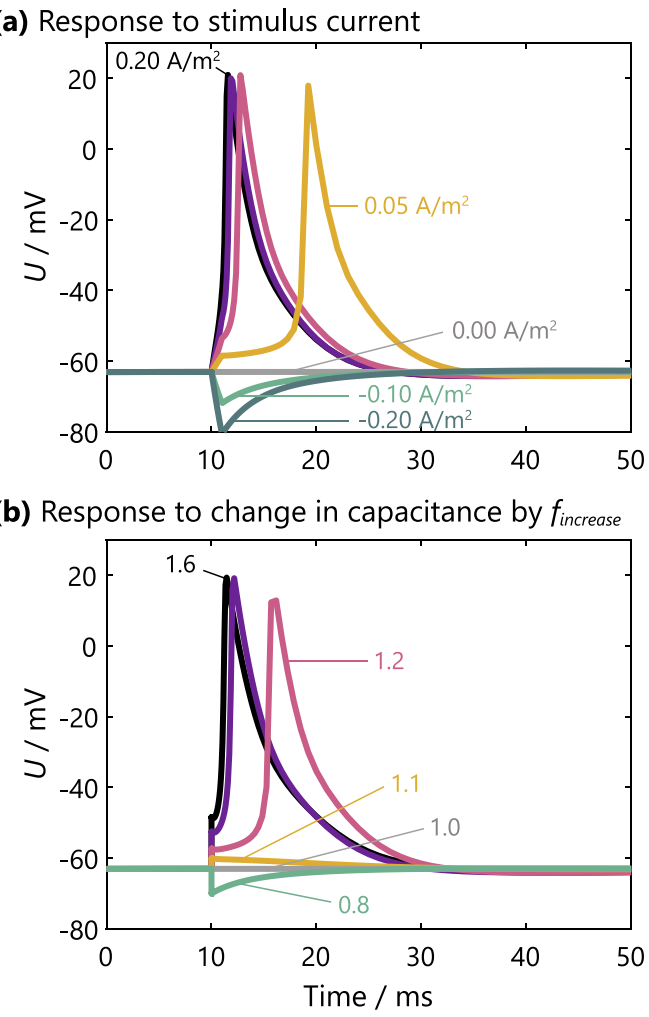

Fig. 7. APs in the equivalent circuit model. (a) APs triggered by conventional external stimulus. Current pulse with duration of 1 ms and amplitude of −0.20, −0.10, 0.00, 0.05, 0.10, 0.15, or 0.20 A/m^2 is applied at time $t = 10$ ms. AP is triggered for amplitudes ≥ 0.05 A/m^2, as indicated in the figure. (b) APs triggered solely by an increase in membrane capacitance due to lipid oxidation. Membrane capacitance is increased by a factor $f_{increase}$ of 0.8, 1.0, 1.1, 1.2, 1.4, or 1.6 at $t = 10$ ms. AP is triggered for $f_{increase} \geq 1.2$, as indicated in the figure. No external stimulus is applied. In this example the non-oxidized and oxidized membrane are considered to have equal area.

again computed the minimum areal fraction of oxidized lesions required to trigger an AP. Table 2 compares this minimum areal fraction when we consider the change in membrane capacitance only, the change in membrane conductance only, and the change in both membrane capacitance and conductance. It turns out that the minimum areal fraction is considerably lower when we also take into account the increase in membrane conductance. Merely 0.2 % lesion area is needed, when the lesions contain 100 % lipid EE13 lipid hydroperoxides, whereas 0.002 % lesion area is needed, when lesions contain 50 % PoxnoPC.

Interestingly, the minimum lesion area is practically identical when we consider the increase in conductance only and both the increase in capacitance and conductance. This means that the change in membrane conductance is actually much more important (i.e. it is the dominant mechanism) for triggering APs compared with the change in membrane capacitance.

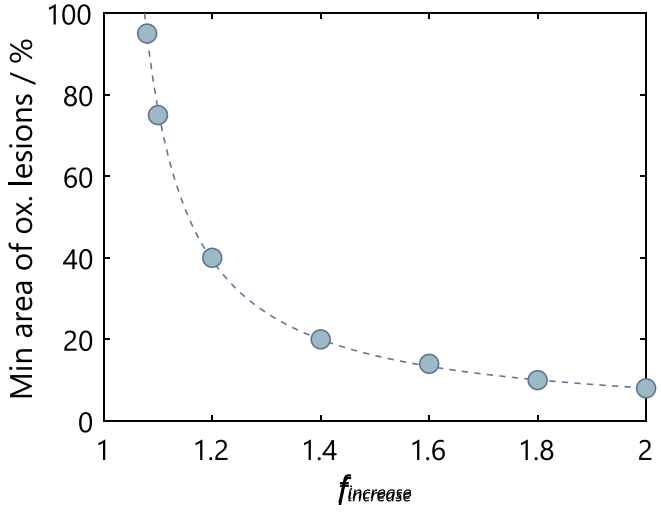

Fig. 8. Minimum areal fraction of oxidized lesions required to trigger an AP, depending on the increase in membrane capacitance upon oxidation, $f_{increase} = C/C_0$. Circles show the results obtained with the equivalent circuit model. Dashed line shows best fit with a rational function $A_{min} = 8.12\ \%/(f_{increase} - 0.99)$.

Table 2
Minimum areal fraction of oxidized lesions in the cell membrane required to trigger an AP. Calculations using the equivalent circuit model are performed for three cases: when considering the change in membrane capacitance only (ΔC), change in membrane conductance only (ΔG), and both change in membrane capacitance and conductance (ΔC & ΔG) due to formation of oxidized lesions. Calculations using the 2D and 3D cell models are performed just for the third case ΔC & ΔG.

Percentage of ox. lipids in a lesion	Lesion properties		Minimum areal fraction to trigger an AP		
	C / C_0	G_{ox} (S/m^2)	Equiv. circuit model (ΔC | ΔG | ΔC & ΔG)	2D cell model with 1 lesion (ΔC & ΔG)	3D cell model with 20 lesions (ΔC & ΔG)
50 % EE13	1.13	0.19	56 % | 25 % | 24 %	20 %	20 %
100 % EE13	1.50	26	15 % | 0.2 % | 0.2 %	0.2 %	0.2 %
10 % PoxnoPC	1.19	0.5	39 % | 10 % | 10 %	8 %	8 %
20 % PoxnoPC	1.24	2	31 % | 2 % | 2 %	2 %	2 %
50 % PoxnoPC	1.82	2000	9 % | 0.003 % | 0.003 %	0.002 %	0.002 %

3.5. Findings are corroborated by the whole-cell model

Finally, we corroborated the results obtained with equivalent circuit model by performing simulations of AP generation at the whole cell level. For simplicity and generality, we considered a spherical cell with a typical radius of 10 μm. Exposure of the cell to 1 ms pulse resulting in electric field ≥ 11 V/cm triggers an AP (Fig. 9a). On the contrary, exposure to a 200 ns, 1–4 kV/cm pulse induces a transmembrane voltage > 0.8 V; however, the pulse is too short to trigger an AP (Fig. 9b). Note, however, that a single 200 ns of ≥ 2.5 kV/cm has been reported to trigger APs in neurons [11].

Similarly as with the equivalent circuit model, we investigated what is the minimum areal fraction of oxidized lesions needed to trigger an AP in the whole-cell model. We first performed simulations with the 2D axisymmetric model considering a single oxidized lesion (Fig. 4a).

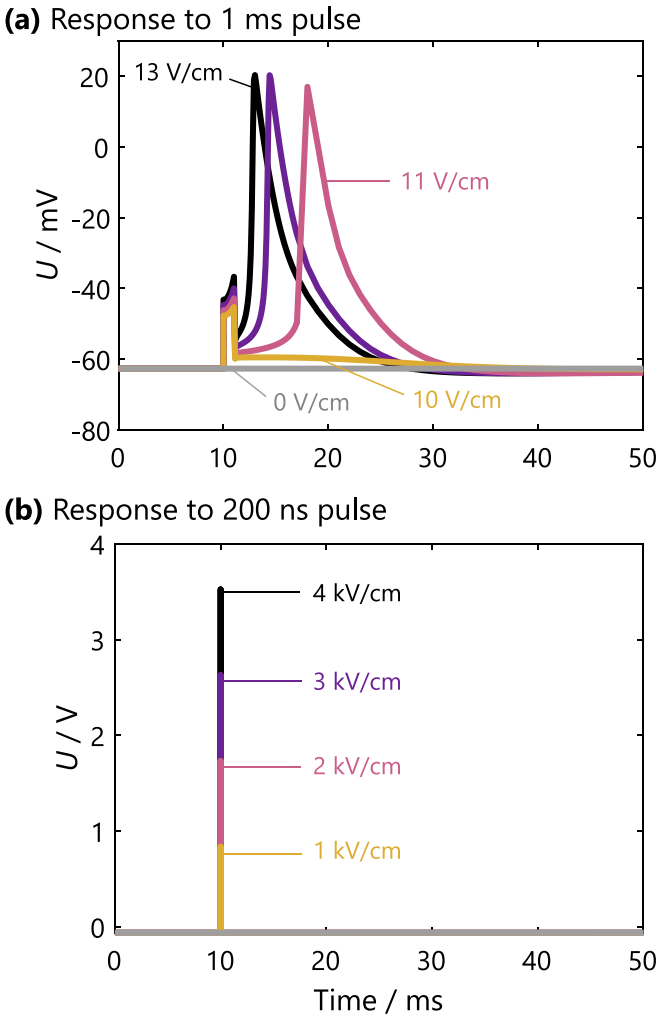

Fig. 9. APs in the whole cell model. (a) Response to a 1-ms-pulse resulting in electric field strength of 0, 10, 11, 12, or 13 V/cm, applied at time $t = 10$ ms. AP is triggered for pulse amplitudes ≥ 11 V/cm, as indicated in the figure. Note that the transmembrane voltage is shown on the depolarized (cathodic) side of the membrane. On the hyperpolarized (anodic) side, the transmembrane voltage during the pulse becomes more negative; however, an AP is still triggered, as the AP is observed along the entire cell membrane. (b) Response to 200-ns-pulse resulting in electric field strength of 0, 1, 2, 3, or 4 kV/cm. The transmembrane voltage reaches > 0.8 V, however, the pulse is too short to trigger an AP.

Table 2 (second to last column) reports the values of the minimum areal fraction of the oxidized lesion needed to trigger an AP. Interestingly, the area obtained with the whole-cell model is almost identical to the one obtained with the equivalent circuit, confirming the robustness of our calculations.

We also performed calculations with the 3D cell model considering 20 randomly distributed oxidized lesions of equal size (Fig. 4b). Despite having multiple lesions instead of one, their summed areal fraction required to trigger an AP is identical to the minimum fraction obtained with the 2D cell model considering a single lesion. Fig. 10 further demonstrates that the generation of APs is the same whether a single or multiple lesions are created, keeping the total lesion area the same.

In all calculations presented so far, we considered a step change in membrane capacitance and/or conductance upon oxidation with no return towards the baseline membrane properties. It is unclear for how long can oxidized lesions persist in a cell membrane before being removed by membrane repair mechanisms, or before they disassemble via lateral diffusion of oxidized lipids. Recent MD study demonstrated

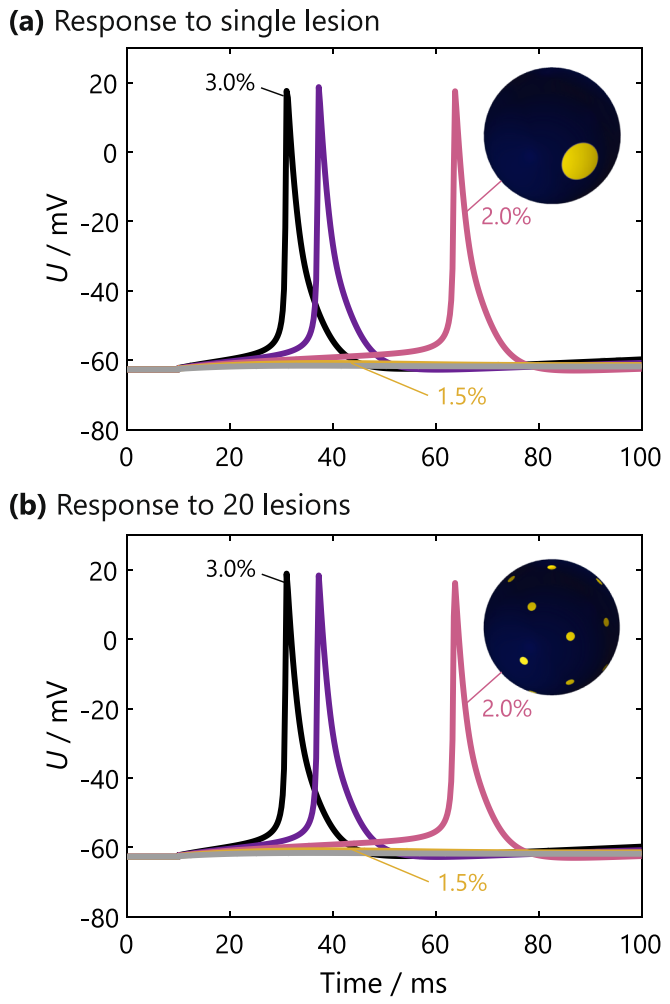

Fig. 10. Response to lipid oxidation in the whole-cell model. As example, lesion(s) consisting of 20 % PoxnoPC are considered to form at time $t = 10$ ms. (a) Response to creation of a single lesion with area of 1.0, 1.5, 2.0, 2.5, or 3.0 % of the cell membrane area. AP triggers for area $\geq$ 2.0 %. (b) Response to creation of 20 lesions with their total (summed) area of 1.0, 1.5, 2.0, 2.5, or 3.0 % of the cell membrane area. The inset in each graph depicts a cell with either (a) single or (b) 20 oxidized lesions (yellow) with the total lesion area accounting for 2.0 % of the cell membrane.

that in pure lipid bilayers, lateral diffusion of oxidized lipids takes place on a time scale of several μs; however, even longer time scales are expected in the cell membrane [39]. Thus, we also computed the minimum areal fraction of oxidized lesions required to trigger an AP when the lesion properties are considered to return exponentially to baseline values with characteristic decay time of t_{lesion}. The results are presented in Fig. 11, where t_{lesion} is varied between 10 μs and 10 s. The shorter the decay time, the larger must be the oxidized area. For instance, for lesions with 50 % PoxnoPC the minimum areal fraction at $t_{lesion} = 10$ μs is 4 % compared with 0.002 % at $t_{lesion} = 100$ ms; for lesions will less PoxnoPC content, APs cannot be fired when $t_{lesion} = 10$ μs.

Lastly, we investigated how creation of oxidized lesions would affect AP generation in conditions of repetitive nsPEF stimulation (Fig. 12). For illustration, we considered that a new lesion with 100 % EE13 lipids forms every second, whereby each lesion occupies 0.2 % total membrane area (just enough for AP generation). We performed calculations for three different values of t_{lesion} (0.1 s, 1 s, and ∞). When $t_{lesion} = 0.1$ s, the membrane properties return to baseline before the next "stimulus" and each creation of a new lesion results in a single AP (Fig. 12a). When $t_{lesion} = 1$ s, the creation of the first lesion results in a single AP, whereas subsequent lesions result in multiple APs (Fig. 12b). Generation of

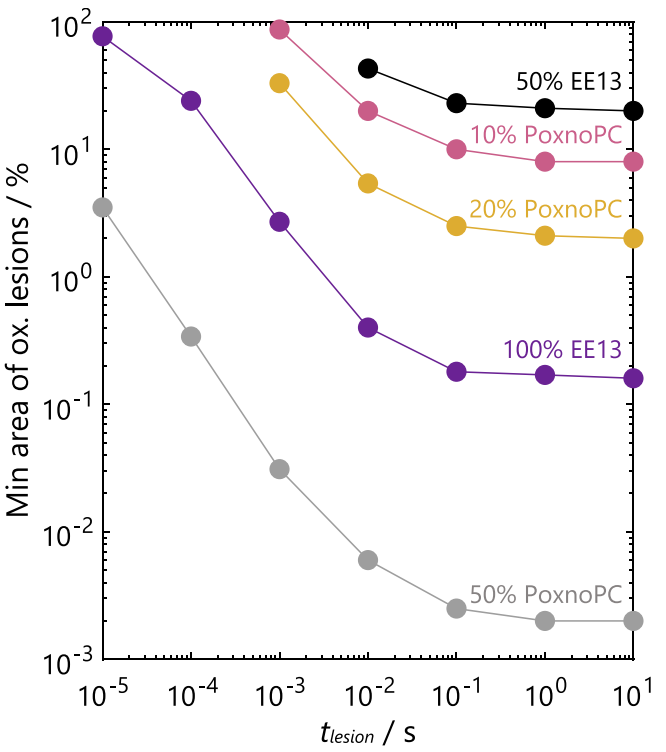

Fig. 11. Minimum areal fraction of oxidized lesions required to trigger an AP, depending on the characteristic decay time t_{lesion}, with which the membrane properties return to baseline value.

multiple APs can be better understood when looking at results for $t_{lesion} = \infty$, i.e., when the lesion properties remain constant over time and each new lesion increases the membrane capacitance and conductance further. In the case presented in Fig. 12c, formation of the second lesion already increases the membrane conductance to an extent that leads to repetitive firing, analogous to repetitive firing in neurons observed under constant injected current. If the accumulated lesions increase the membrane conductance further, we can eventually see sustained membrane depolarization with no APs (see last two segments in Fig. 12c).

4. Discussion

In this study we demonstrated that formation of oxidized membrane lesions, promoted by exposure to nsPEFs, could trigger an AP due to local membrane depolarization caused by a change in bilayer capacitance and conductance.

4.1. Oxidized lipids increase both membrane capacitance and conductance

We first prepared molecular models of bilayers containing different percentage of primary or secondary lipid oxidation products and used MD simulations to determine the specific membrane capacitance. We observed that the capacitance increases with increasing percentage of oxidized lipids up to a factor of ~2 with respect to the capacitance of a non-oxidized bilayer. Lipid oxidation introduces polar and hydrophilic groups (i.e., hydroperoxide, aldehyde, or carbonyl groups) into the hydrocarbon lipid chain inside the bilayer. Ours and others' previous studies demonstrated that the presence of OOH and CH=O groups affects the properties of a lipid bilayer in several ways: increases the area per lipid, decreases the bilayer thickness, decreases the bilayer dipole potential, decreases lipid order parameters, increases the water permeability, promotes transient water defects at the lipid-water interface, etc. [58,59,38,39]. The presence of polar groups in the hydrocarbon chain,

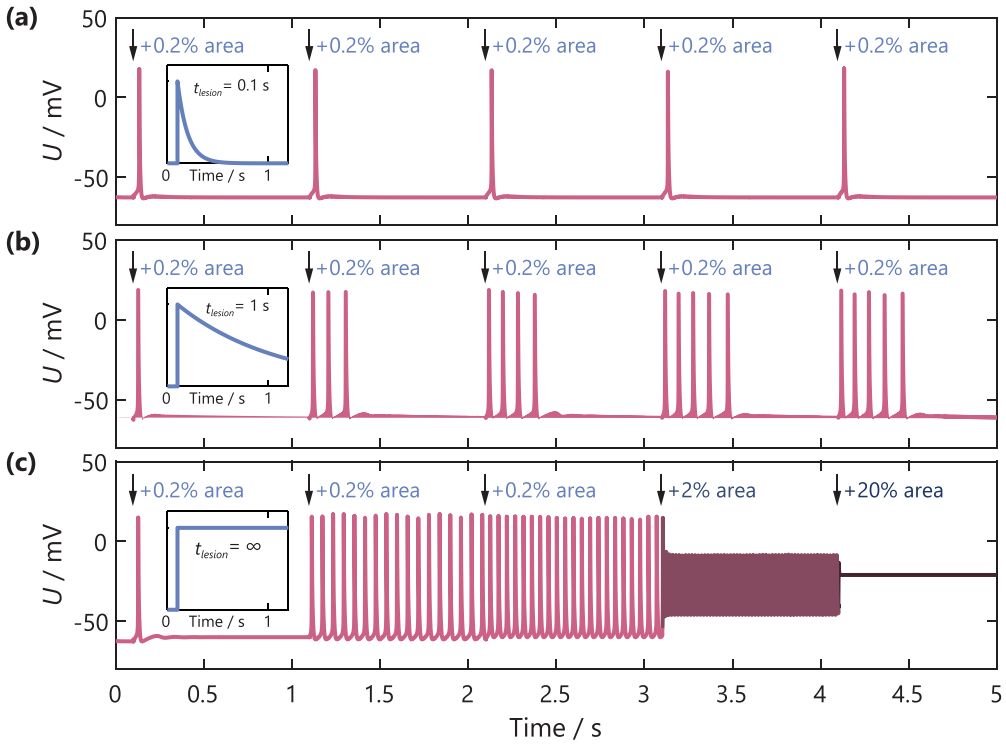

Fig. 12. Response to repetitive lesion formation in the whole-cell model. A lesion with 100 % EE13 lipids forms every second (see arrows), whereby each lesion occupies 0.2 % total membrane area. Calculations are performed for three values of t_{lesion}: 0.1 s (a), 1 s (b), and ∞ (c). Insets show the time course of the lesion properties (capacitance and conductance). The last two segments in (c) are computed for greater lesion size (2 % and 20 % of the total membrane area).

together with greater water content inside the bilayer and greater lipid mobility, makes the membrane more dielectrically polarizable, i.e., increases its dielectric permittivity. Greater dielectric permittivity and reduced membrane thickness are then reflected in the increased specific membrane capacitance [60].

Recent measurements in planar lipid bilayers confirmed that the presence of various types of oxidized lipids increases the bilayer capacitance [61]. An increase in capacitance was also experimentally observed after exposing membranes to ionizing radiation [62] or photodynamic treatment [63]. Ionizing radiation is known to induce the radiolysis of water and so to be a source of ROS. The increase in membrane capacitance was found to depend on the presence of unsaturated lipid in the membrane and, therefore, to be directly linked with lipid oxidation. Similarly, following photodynamic treatment, a light-induced increase in the capacitance was observed, but only for the unsaturated lipid and in the presence of a sensitizer [63]. The presence of scavengers or antioxidants inhibited (partially or totally) the response. It is important to stress that in all these experimental studies, the increase in membrane capacitance was correlated with an increase in membrane conductance, which is consistent with our previous characterization of bilayer conductance in the same model systems as used in this study (see also Table 2). Creation of an oxidized membrane lesion thus increases simultaneously both the local membrane capacitance and conductance.

4.2. Creation of oxidized lesions in the membrane can trigger an action potential

We hypothesized that a local increase in membrane capacitance and/or conductance due to formation of oxidized lesions could locally depolarize the membrane enough to trigger an AP in excitable cells. An AP is a brief and abrupt depolarization of the membrane due to the opening of VGICs, allowing the ions to pass along their electrochemical gradient. The bilayer models used in MD simulations are aimed to represent a hypothetical environment of the channel. Indeed, the models with all lipids oxidized (100 % EE13 and 100 % PoxnoPC) represent a part of a fully oxidized cell membrane lesion. Such lesion can be the consequence of the propagation of oxidative damage from one unsaturated lipid to the surrounding lipids, forming a patch. But such lesion can also be formed by local aggregation (clustering) of oxidized lipids. Moreover, the models made of a homogenous mixture of oxidized and non-oxidized lipids represent lesions in the membrane, where polyunsaturated lipids represent a fraction of the lipid mixture, or lesions where the oxidized lipids have diffused away from the original lesion. The lateral diffusion of oxidized lipids out of the original lesion is a μs-scale or longer phenomenon [39]. Hence, oxidized lesions are expected to persist on a longer time scale than the duration of a pulse used in nsPEF stimulation.

For systematic purposes, we first investigated whether solely the increase in membrane capacitance (without increased membrane conductance) would be sufficient to activate Na_V channels and trigger an AP, as suggested by our simple calculation based on $U = Q/C$ relationship (Fig. 6). Indeed, both our Hodgkin-Huxley-type equivalent circuit and whole-cell finite-element models showed that APs can be triggered by a change in membrane capacitance, provided that a sufficient fraction (at least ~10 %) of the total cell membrane area becomes oxidized. It needs to be stressed that it is the dynamic change in membrane capacitance that depolarizes the membrane to a sufficient extent to trigger an AP. In steady state, the altered value of the membrane capacitance has no influence on the transmembrane voltage. This is reflected, e.g., by the Goldman-Hodgkin-Katz equation, which describes how the resting transmembrane voltage depends on the intracellular and extracellular concentrations of ions and the membrane permeability for these ions. The Goldman-Hodgkin-Katz equation does not include the membrane capacitance, since the steady state transmembrane voltage is independent of its value.

We next investigated how the local increase in membrane conductance, which accompanies the increase in membrane capacitance inside oxidized lesions, affects AP initiation. It turned out that an AP could be

triggered solely by the increase in membrane conductance without any change in membrane capacitance (Table 2). In fact, the increase in membrane conductance is the dominant mechanism contributing to AP initiation and is much more important than the increase in membrane capacitance. When considering lesions containing 50 % secondary oxidation products (PoxnoPC lipids), and taking into account both the increase in membrane capacitance and conductance, as little as 0.002 % of the membrane area needs to be oxidized for triggering an AP. It does not matter whether a single lesion of this area or multiple lesions of the same summed area are formed (Fig. 10). In other words, multiple lesions created simultaneously contribute to initiation of an AP in a similar way as a single larger lesion. In analogy, initiation of an AP in a neuron is also based on a sum of multiple subthreshold excitatory postsynaptic potentials, whereby it is their summation that reaches the threshold and enables AP activation in the axon initial segment.

4.3. Accumulation of oxidized lesions can alter cellular excitability and AP generation

However, the duration for which the lesion(s) exists has an important influence on AP generation. On the one hand, the shorter the lifetime of the lesion, the greater the fraction of the cell membrane area that needs to be oxidized to trigger an AP (Fig. 11). On the other hand, the longer the lesion lifetime, the more the lesions can accumulate over time under conditions of repetitive electrostimulation (Fig. 12). Our results demonstrate that such accumulation of lesions can increase the membrane conductance to an extent that alters cellular excitability and AP generation. Intermediate increase in membrane conductance can lead to periodic generation of APs, which is analogous to periodic firing of neurons under constant current stimulus. Higher increase in membrane conductance leads to sustained membrane depolarization with no APs (Fig. 12c). Whether periodic generation of APs can be observed experimentally will depend on the electrophysiological characteristics of a given excitable cell type and its ability to shift into an oscillatory mode. In experiments with excitable cells exposed to nsPEF (and longer pulses) it has been observed that repetitive stimulation can lead to oscillations in intracellular calcium in isolated cardiomyocytes [64,65], where these oscillations are likely linked with oscillations in the transmembrane voltage. Moreover, sustained membrane depolarization following exposure to intense nsPEF has been observed in primary neurons [66]. Note that altered cell excitability, associated with an increase in membrane conductance, has also been observed following exposure of cardiomyocytes to longer electric pulses with amplitudes above the electrostimulation threshold [67,68].

4.4. Alternative mechanisms leading to an increase in membrane conductance could also lead to AP activation

We initiated this study with the hypothesis that formation of oxidized lesions could trigger an AP due to a local increase in membrane capacitance, whereas our modeling results demonstrated that it is the associated local increase in membrane conductance that is the main mechanism leading to AP activation. Nevertheless, an increase in membrane conductance after nsPEF exposure could also be due to mechanisms alternative to lipid oxidation. It has been long known that nsPEFs of high enough magnitude (order of 1–100 kV/cm, depending on the pulse duration) can induce formation of pores in the lipid domains of the cell membrane [22,69,70]. However, such lipid pores are expected to close within tens to hundreds of nanoseconds, as predicted by MD simulations [71–73] and experiments on lipid vesicles [74]. The nanosecond lifetime of lipid pores makes them unlikely candidate for VGICs activation. Recent MD studies [23,75] suggested that pores can as well form in the voltage sensor domains of VGICs, when the latter are exposed to nsPEFs. Extensive MD simulations indicated that these pores, which become stabilized by both lipid and amino acid residues, are more stable than the “classic” lipid pores and could better explain the long-lived increase in membrane permeability following nsPEF observed experimentally [23]. It was also noted that ultimately, these defects are likely to cause the VGIC to become rather insensitive to transmembrane voltage changes, and unable to function. However, provided that only a small subset of VGICs becomes dysfunctional by nsPEF, the increase in membrane conductance resulting from these denatured channels could nevertheless enable activation of the unperturbed Na_V channels and AP initiation. Furthermore, membrane proteins other than VGICs could become damaged and thereby contribute to the increased membrane conductance [76,77]. In addition, activation of other ion channels, such as transient receptor potential channels, sodium leak channels, or calcium-dependent potassium channels, could contribute to the increased membrane conductance and observed response of excitable cells following nsPEF exposure [78,79].

5. Conclusions

In summary, our study suggests that formation of oxidized lipid lesions in the membrane, induced by nsPEF, could result in AP activation, due to local change in membrane electrical properties, particularly an increase in local membrane conductance. However, accumulation of oxidative lesions could increase the membrane conductance to an extent that alters cellular excitability and even inhibits AP generation. Further research, including patch-clamp measurements of the changes in membrane capacitance upon nsPEF exposure, structural studies on membrane protein perturbation, and studies probing the kinetics of lateral diffusion of oxidized lipids as well as their replacement by the cell (membrane repair mechanisms), can help decipher the underlying mechanism of AP triggering by nsPEFs. While we primarily focused our discussion on nsPEFs, we note that lipid oxidation generally takes place also with more conventional microsecond and millisecond electroporation pulses. Therefore, we expect that lipid oxidation (as well as other molecular mechanisms leading to increased membrane conductance) can influence cellular excitability in a wide range of electroporation-based applications, including ablation of brain tumors and epileptic zones [80,81], ablation of arrhythmogenic cardiac tissue [82,83], and gene electrotransfer to skeletal muscles [84].

Declaration of Competing Interest

The authors declare that they have no known competing financial interests or personal relationships that could have appeared to influence the work reported in this paper.

Data availability

FEM models developed in the study ara available at https://github.com/learems/Oxidation-Excitation. Molecular dynamics simulations data will be made available upon request.

Acknowledgments

High Performance Computing resources have been provided by the EXPLOR center hosted by the University de Lorraine (project 2018PMXX0420). AR acknowledges the support from Lorraine Université d’Excellence for a PhD Fellowship. We acknowledge financial support from Partenariat Hubert Curien PROTEUS 22 and from Slovenian Research Agency (ARRS research programme P2-0249 and projects no. J2-2503 and BI-FR/22-23-PROTEUS-006). This work was also supported by funding from the European Union’s Horizon 2020 research and innovation program under the Marie Skłodowska-Curie grant agreement No. 893077 (to LR). LR thanks Janja Dermol-Černe for initial help with Hodgkin-Huxley models and Damijan Miklavčič for useful comments to the manuscript.

Appendix A. Supplementary data

Supplementary data to this article can be found online at https://doi.org/10.1016/j.bioelechem.2023.108588.

References

[1] M. Madhavan, S.K. Mulpuru, C.J. McLeod, Y.-M. Cha, P.A. Friedman, Advances and future directions in cardiac pacemakers, J. Am. Coll. Cardiol. 69 (2017) 211–235, https://doi.org/10.1016/j.jacc.2016.10.064.

[2] C.D. Swerdlow, G. Kalahasty, K.A. Ellenbogen, Implantable cardiac defibrillator lead failure and management, J. Am. Coll. Cardiol. 67 (2016) 1358–1368, https://doi.org/10.1016/j.jacc.2015.12.067.

[3] J. Schoenen, R. Baschi, D. Magis, G. Coppola, Noninvasive neurostimulation methods for migraine therapy: The available evidence, Cephalalgia 36 (2016) 1170–1180, https://doi.org/10.1177/0333102416636022.

[4] X. Moisset, B. Pereira, D. Ciampi de Andrade, D. Fontaine, M. Lantéri-Minet, J. Mawet, Neuromodulation techniques for acute and preventive migraine treatment: A systematic review and meta-analysis of randomized controlled trials, J. Headache Pain 21 (2020), https://doi.org/10.1186/s10194-020-01204-4.

[5] K.S. Chen, R. Chen, Invasive and noninvasive brain stimulation in parkinson's disease: Clinical effects and future perspectives, Clin. Pharmacol. Ther. 106 (2019) 763–775, https://doi.org/10.1002/cpt.1542.

[6] T.J. Foutz, M. Wong, Brain stimulation treatments in epilepsy: Basic mechanisms and clinical advances, Biomedical Journal. 45 (2022) 27–37, https://doi.org/10.1016/j.bj.2021.08.010.

[7] C. Burton, A. Sajja, P.M. Latthe, Effectiveness of percutaneous posterior tibial nerve stimulation for overactive bladder: A systematic review and meta-analysis, Neurourol. Urodyn. 31 (2012) 1206–1216, https://doi.org/10.1002/nau.22251.

[8] J.U. Neuber, F. Varghese, A.G. Pakhomov, C.W. Zemlin, Using nanosecond shocks for cardiac defibrillation, Bioelectricity. 1 (2019) 240–246, https://doi.org/10.1089/bioe.2019.0030.

[9] A.G. Pakhomov, E. Gudvangen, S. Xiao, I. Semenov, Interference targeting of bipolar nanosecond electric pulses for spatially focused electroporation, electrostimulation, and tissue ablation, Bioelectrochemistry 141 (2021) 107876, https://doi.org/10.1016/j.bioelechem.2021.107876.

[10] N. Jiang, B.Y. Cooper, Frequency-dependent interaction of ultrashort E-fields with nociceptor membranes and proteins, Bioelectromagnetics 32 (2011) 148–163, https://doi.org/10.1002/bem.20620.

[11] A.G. Pakhomov, I. Semenov, M. Casciola, S. Xiao, Neuronal excitation and permeabilization by 200-ns pulsed electric field: An optical membrane potential study with FluoVolt dye, Biochim. Biophys. Acta Biomembr. 2017 (1859) 1273–1281, https://doi.org/10.1016/j.bbamem.2017.04.016.

[12] M. Casciola S. Xiao A.G. Pakhomov Damage-free peripheral nerve stimulation by 12-ns pulsed electric field Scientific Reports. 2017 1 8 10.1038/s41598-017-10282-5.

[13] M. Casciola, S. Xiao, F. Apollonio, A. Paffi, M. Liberti, C. Muratori, A.G. Pakhomov, Cancellation of nerve excitation by the reversal of nanosecond stimulus polarity and its relevance to the gating time of sodium channels, Cell. Mol. Life Sci. 76 (2019) 4539–4550, https://doi.org/10.1007/s00018-019-03126-0.

[14] A.G. Pakhomov, S. Xiao, V. Novickij, M. Casciola, I. Semenov, U. Mangalanathan, V. Kim, C. Zemlin, E. Sozer, C. Muratori, O.N. Pakhomova, Excitation and electroporation by MHz bursts of nanosecond stimuli, Biochem. Biophys. Res. Commun. 518 (2019) 759–764, https://doi.org/10.1016/j.bbrc.2019.08.133.

[15] I. Semenov, S. Grigoryev, J.U. Neuber, C.W. Zemlin, O.N. Pakhomova, M. Casciola, A.G. Pakhomov, Excitation and injury of adult ventricular cardiomyocytes by nano- to millisecond electric shocks, Sci. Rep. 8 (2018) 8233, https://doi.org/10.1038/s41598-018-26521-2.

[16] J.E. Azarov, I. Semenov, M. Casciola, A.G. Pakhomov, Excitation of murine cardiac myocytes by nanosecond pulsed electric field, J. Cardiovasc. Electrophysiol. 30 (2019) 392–401, https://doi.org/10.1111/jce.13834.

[17] P.T. Vernier, Y. Sun, M.T. Chen, M.A. Gundersen, G.L. Craviso, Nanosecond electric pulse-induced calcium entry into chromaffin cells, Bioelectrochemistry 73 (2008) 1–4, https://doi.org/10.1016/j.bioelechem.2008.02.003.

[18] G.L. Craviso, S. Choe, P. Chatterjee, I. Chatterjee, P.T. Vernier, Nanosecond electric pulses: A novel stimulus for triggering Ca2+ influx into chromaffin cells via voltage-gated Ca2+ channels, Cell. Mol. Neurobiol. 30 (2010) 1259–1265, https://doi.org/10.1007/s10571-010-9573-1.

[19] T.R. Bagalkot, R.C. Terhune, N. Leblanc, G.L. Craviso, Different membrane pathways mediate Ca2+ influx in adrenal chromaffin cells exposed to 150–400 ns electric pulses, Biomed Res. Int. 2018 (2018), https://doi.org/10.1155/2018/9046891.

[20] Y. Wang, D. DeMazumder, J.A. Hill, Chapter 7 - Ionic Fluxes and Genesis of the Cardiac Action Potential, in: J.A. Hill, E.N. Olson (Eds.), Muscle, Academic Press, Boston/Waltham, 2012, pp. 67–85, https://doi.org/10.1016/B978-0-12-381510-1.00007-7.

[21] A. Fletcher, Action potential: Generation and propagation, Anaesthesia & Intensive Care Medicine. 17 (2016) 204–208, https://doi.org/10.1016/j.mpaic.2016.01.006.

[22] T. Kotnik, L. Rems, M. Tarek, D. Miklavčič, Membrane electroporation and electropermeabilization: Mechanisms and models, Annu. Rev. Biophys. 48 (2019) 63–91, https://doi.org/10.1146/annurev-biophys-052118-115451.

[23] L. Rems, M.A. Kasimova, I. Testa, L. Delemotte, Pulsed electric fields can create pores in the voltage sensors of voltage-gated ion channels, Biophys. J . (2020) 1–22, https://doi.org/10.1016/j.bpj.2020.05.030.

[24] A.G. Pakhomov, O.N. Pakhomova, The interplay of excitation and electroporation in nanosecond pulse stimulation, Bioelectrochemistry 136 (2020) 107598, https://doi.org/10.1016/j.bioelechem.2020.107598.

[25] R. Nuccitelli, K. Lui, M. Kreis, B. Athos, P. Nuccitelli, Nanosecond pulsed electric field stimulation of reactive oxygen species in human pancreatic cancer cells is Ca2+-dependent, Biochemical and Biophysical Research Communications. 435 (2013) 580–585, https://doi.org/10.1016/j.bbrc.2013.05.014.

[26] O.N. Pakhomova, V.A. Khorokhorina, A.M. Bowman, R. Rodaitė-Riševičienė, G. Saulis, S. Xiao, A.G. Pakhomov, Oxidative effects of nanosecond pulsed electric field exposure in cells and cell-free media, Arch. Biochem. Biophys. 527 (2012) 55–64, https://doi.org/10.1016/j.abb.2012.08.004.

[27] R.M. Cordeiro, Reactive oxygen species at phospholipid bilayers: Distribution, mobility and permeation, Biochimica et Biophysica Acta (BBA) - Biomembranes 1838 (2014) 438–444, https://doi.org/10.1016/j.bbamem.2013.09.016.

[28] A. Reis, C.M. Spickett, Chemistry of phospholipid oxidation, Biochimica et Biophysica Acta - Biomembranes 2012 (1818) 2374–2387, https://doi.org/10.1016/j.bbamem.2012.02.002.

[29] R. Domínguez, M. Pateiro, M. Gagaoua, F.J. Barba, W. Zhang, J.M. Lorenzo, A comprehensive review on lipid oxidation in meat and meat products, Antioxidants. 8 (2019) 1–31, https://doi.org/10.3390/antiox8100429.

[30] L.C. Benov, P.A. Antonov, S.R. Ribarov, Oxidative damage of the membrane lipids after electroporation, Gen. Physiol. Biophys. 13 (1994) 85–97.

[31] B. Gabriel, J. Teissié, Generation of reactive-oxygen species induced by electropermeabilization of Chinese hamster ovary cells and their consequence on cell viability, Eur. J. Biochem. 223 (1994) 25–33, https://doi.org/10.1111/j.1432-1033.1994.tb18962.x.

[32] M. Maccarrone, N. Rosato, A.F. Agrò, Electroporation enhances cell membrane peroxidation and luminescence, Biochem. Biophys. Res. Commun. 206 (1995) 238–245, https://doi.org/10.1006/bbrc.1995.1033.

[33] M. Maccarrone, M.R. Bladergroen, N. Rosato, A.F. Agrò, Role of lipid peroxidation in electroporation-induced cell permeability, Biochemical and Biophysical Research Communications. 209 (1995) 417–425, https://doi.org/10.1006/bbrc.1995.1519.

[34] Y. Zhou, C.K. Berry, P.A. Storer, R.M. Raphael, Peroxidation of polyunsaturated phosphatidyl-choline lipids during electroformation, Biomaterials 28 (2007) 1298–1306, https://doi.org/10.1016/j.biomaterials.2006.10.016.

[35] M. Breton, M. Amirkavei, L.M. Mir, Optimization of the electroformation of giant unilamellar vesicles (GUVs) with unsaturated phospholipids, J. Membr. Biol. 248 (2015) 827–835, https://doi.org/10.1007/s00232-015-9828-3.

[36] O. Michel, A.G. Pakhomov, M. Casciola, J. Saczko, J. Kulbacka, O.N. Pakhomova, Electropermeabilization does not correlate with plasma membrane lipid oxidation, Bioelectrochemistry 132 (2020) 107433, https://doi.org/10.1016/j.bioelechem.2019.107433.

[37] Z.A.M. Zielinski, D.A. Pratt, Lipid Peroxidation: Kinetics, mechanisms, and products, J. Org. Chem. 82 (2017) 2817–2825, https://doi.org/10.1021/acs.joc.7b00152.

[38] L. Rems, M. Viano, M.A. Kasimova, D. Miklavčič, M. Tarek, The contribution of lipid peroxidation to membrane permeability in electropermeabilization: A molecular dynamics study, Bioelectrochemistry (2019), https://doi.org/10.1016/j.bioelechem.2018.07.018.

[39] D. Wiczew, N. Szulc, M. Tarek, Molecular dynamics simulations of the effects of lipid oxidation on the permeability of cell membranes, Bioelectrochemistry 141 (2021) 107869, https://doi.org/10.1016/j.bioelechem.2021.107869.

[40] J.B. Klauda, R.M. Venable, J.A. Freites, J.W. O'Connor, D.J. Tobias, C. Mondragon-Ramirez, I. Vorobyov, A.D. MacKerell, R.W. Pastor, Update of the CHARMM all-atom additive force field for lipids: Validation on Six lipid types, J. Phys. Chem. B 114 (2010) 7830–7843, https://doi.org/10.1021/jp101759q.

[41] J. Garrec, A. Monari, X. Assfeld, L.M. Mir, M. Tarek, Lipid peroxidation in membranes: The peroxyl radical does not "float", J. Phys. Chem. Lett. 5 (2014) 1653–1658, https://doi.org/10.1021/jz500502q.

[42] M.J. Abraham, T. Murtola, R. Schulz, S. Páll, J.C. Smith, B. Hess, E. Lindahl, GROMACS: High performance molecular simulations through multi-level parallelism from laptops to supercomputers, SoftwareX. 1–2 (2015) 19–25, https://doi.org/10.1016/J.SOFTX.2015.06.001.

[43] T. Darden, D. York, L. Pedersen, Particle mesh Ewald: An N·log(N) method for Ewald sums in large systems, J. Chem. Phys. 98 (1993) 10089–10092, https://doi.org/10.1063/1.464397.

[44] U. Essmann, L. Perera, M.L. Berkowitz, T. Darden, H. Lee, L.G. Pedersen, A smooth particle mesh Ewald method, J. Chem. Phys. 103 (1995) 8577–8593, https://doi.org/10.1063/1.470117.

[45] B. Hess, H. Bekker, H.J.C. Berendsen, J.G.E.M. Fraaije, LINCS: A linear constraint solver for molecular simulations, J. Comput. Chem. 18 (1997) 1463–1472, https://doi.org/10.1002/(SICI)1096-987X(199709)18:12<1463::AID-JCC4>3.0.CO;2-H.

[46] M. Parrinello, A. Rahman, Polymorphic transitions in single crystals: A new molecular dynamics method, J. Appl. Phys. 52 (1981) 7182–7190, https://doi.org/10.1063/1.328693.

[47] S. Nosé, A unified formulation of the constant temperature molecular dynamics methods, J. Chem. Phys. 81 (1984) 511–519, https://doi.org/10.1063/1.447334.

[48] W.G. Hoover, Canonical dynamics: Equilibrium phase-space distributions, Phys. Rev. A 31 (1985) 1695–1697, https://doi.org/10.1103/PhysRevA.31.1695.

[49] L. Delemotte, F. Dehez, W. Treptow, M. Tarek, Modeling membranes under a transmembrane potential, J. Phys. Chem. B 112 (2008) 5547–5550, https://doi.org/10.1021/jp710846y.

[50] L. Delemotte, M. Tarek, Molecular dynamics simulations of lipid membrane electroporation, J. Membr. Biol. 245 (2012) 531–543, https://doi.org/10.1007/s00232-012-9434-6.
[51] A.L. Hodgkin, A.F. Huxley, A quantitative description of membrane current and its application to conduction and excitation in nerve, J. Physiol. 117 (1952) 500–544, https://doi.org/10.1113/jphysiol.1952.sp004764.
[52] W. Gerstner, W.M. Kistler, R. Naud, L. Paninski, Neuronal dynamics: from single neurons to networks and models of cognition, UK ed. edition,, Cambridge University Press, Cambridge, United Kingdom, 2014.
[53] D. Boinagrov, J. Loudin, D. Palanker, Strength-duration relationship for extracellular neural stimulation: Numerical and analytical models, J. Neurophysiol. 104 (2010) 2236–2248, https://doi.org/10.1152/jn.00343.2010.
[54] G. Pucihar, D. Miklavčič, T. Kotnik, A time-dependent numerical model of transmembrane voltage inducement and electroporation of irregularly shaped cells, IEEE Trans. Biomed. Eng. 56 (2009) 1491–1501, https://doi.org/10.1109/TBME.2009.2014244.
[55] L. Rems, M. Ušaj, M. Kandušer, M. Reberšek, D. Miklavčič, G. Pucihar, Cell electrofusion using nanosecond electric pulses, Sci. Rep. 3 (2013) 3382, https://doi.org/10.1038/srep03382.
[56] M. Scuderi, J. Dermol-Černe, C. Amaral da Silva, A. Muralidharan, P.E. Boukany, L. Rems, Models of electroporation and the associated transmembrane molecular transport should be revisited, Bioelectrochemistry 147 (2022) 108216, https://doi.org/10.1016/j.bioelechem.2022.108216.
[57] S.K. Abbott, P.L. Else, T.A. Atkins, A.J. Hulbert, Fatty acid composition of membrane bilayers: Importance of diet polyunsaturated fat balance, Biochimica et Biophysica Acta (BBA) - Biomembranes 1818 (2012) 1309–1317, https://doi.org/10.1016/j.bbamem.2012.01.011.
[58] J. Wong-ekkabut, Z. Xu, W. Triampo, I.-M. Tang, D.P. Tieleman, L. Monticelli, Effect of lipid peroxidation on the properties of lipid bilayers: A molecular dynamics study, Biophys. J . 93 (2007) 4225–4236, https://doi.org/10.1529/biophysj.107.112565.
[59] P. Boonnoy, V. Jarerattanachat, M. Karttunen, J. Wong-ekkabut, Bilayer deformation, pores, and micellation induced by oxidized lipids, J. Phys. Chem. Lett. (2015) 4884–4888, https://doi.org/10.1021/acs.jpclett.5b02405.
[60] G. Stark, The effect of ionizing radiation on lipid membranes, Biochim. Biophys. Acta 1071 (1991) 103–122, https://doi.org/10.1016/0304-4157(91)90020-w.
[61] K. Balantič, V.U. Weiss, E. Pittenauer, D. Miklavčič, P. Kramar, The role of lipid oxidation on electrical properties of planar lipid bilayers and its importance for understanding electroporation, Bioelectrochemistry 153 (2023) 108498, https://doi.org/10.1016/j.bioelechem.2023.108498.
[62] M. Strässle, M. Wilhelm, G. Stark, The increase of membrane capacitance as a consequence of radiation-induced lipid peroxidation, Int. J. Radiat Biol. 59 (1991) 71–83, https://doi.org/10.1080/09553009114550071.
[63] F. Killig, G. Stark, Photodynamic activation of ion transport through lipid membranes and its correlation with an increased dielectric constant of the membrane, Biochimica et Biophysica Acta - Biomembranes 1564 (2002) 207–213, https://doi.org/10.1016/S0005-2736(02)00452-2.
[64] I. Semenov, S. Xiao, O.N. Pakhomova, A.G. Pakhomov, Recruitment of the intracellular Ca2+ by ultrashort electric stimuli: The impact of pulse duration, Cell Calcium 54 (2013) 145–150, https://doi.org/10.1016/j.ceca.2013.05.008.
[65] S. Chaigne, D.C. Sigg, M.T. Stewart, M. Hocini, B. Napotnik, D. Miklavcic, O. Bernus, D. Benoist, Reversible and irreversible effects of electroporation on contractility and calcium homeostasis in isolated cardiac ventricular myocytes, Circ.: Arrhythmia Electrophysiol. 15 (2022), e011131, https://doi.org/10.1161/circep.122.011131.
[66] A.G. Pakhomov, I. Semenov, M. Casciola, S. Xiao, Neuronal excitation and permeabilization by 200-ns pulsed electric field: An optical membrane potential study with FluoVolt dye, Biochim. Biophys. Acta (BBA) - Biomembranes. 1859 (2017) 1273–1281, https://doi.org/10.1016/j.bbamem.2017.04.016.
[67] L. Tung, O. Tovar, M. Neunlist, S.K. Jain, R.J. O'Neill, Effects of strong electrical shock on cardiac muscle tissue, Ann. N. Y. Acad. Sci. 720 (1994) 160–175, https://doi.org/10.1111/j.1749-6632.1994.tb30444.x.
[68] M. Neunlist, L. Tung, Dose-dependent reduction of cardiac transmembrane potential by high-intensity electrical shocks, American Journal of Physiology-Heart and Circulatory Physiology 273 (1997) H2817–H2825, https://doi.org/10.1152/ajpheart.1997.273.6.H2817.
[69] A.G. Pakhomov, R. Shevin, J.A. White, J.F. Kolb, O.N. Pakhomova, R.P. Joshi, K. H. Schoenbach, Membrane permeabilization and cell damage by ultrashort electric field shocks, Arch. Biochem. Biophys. 465 (2007) 109–118, https://doi.org/10.1016/j.abb.2007.05.003.
[70] I. Semenov, S. Xiao, A.G. Pakhomov, Electroporation by subnanosecond pulses, Biochem. Biophys. Rep. 6 (2016) 253–259, https://doi.org/10.1016/j.bbrep.2016.05.002.
[71] M. Tarek, Membrane electroporation: A molecular dynamics simulation, Biophys. J . 88 (2005) 4045–4053, https://doi.org/10.1529/biophysj.104.050617.
[72] W.F.D. Bennett, N. Sapay, D.P. Tieleman, Atomistic simulations of pore formation and closure in lipid bilayers, Biophys. J. 106 (2014) 210–219, https://doi.org/10.1016/j.bpj.2013.11.4486.
[73] Z.A. Levine, P.T. Vernier, Life cycle of an electropore: Field-dependent and field-independent steps in pore creation and annihilation, J. Membr. Biol. 236 (2010) 27–36, https://doi.org/10.1007/s00232-010-9277-y.
[74] E.B. Sözer, S. Haldar, P.S. Blank, F. Castellani, P.T. Vernier, J. Zimmerberg, Dye transport through bilayers agrees with lipid electropore molecular dynamics, Biophys. J. 119 (2020) 1724–1734, https://doi.org/10.1016/j.bpj.2020.09.028.
[75] A.R. Ruiz-Fernández, L. Campos, F. Villanelo, S.E. Gutiérrez-Maldonado, T. Perez-Acle, Exploring the conformational changes induced by nanosecond pulsed electric fields on the voltage sensing domain of a Ca2+ channel, Membranes 11 (2021) 473, https://doi.org/10.3390/membranes11070473.
[76] J. Teissié, T.Y. Tsong, Evidence of voltage-induced channel opening in Na/K ATPase of human erythrocyte membrane, J. Membrain Biol. 55 (1980) 133–140, https://doi.org/10.1007/BF01871155.
[77] G. Silkuniene, U.M. Mangalanathan, A. Rossi, P.A. Mollica, A.G. Pakhomov, O. Pakhomova, Identification of proteins involved in cell membrane permeabilization by nanosecond electric pulses (nsEP), Int. J. Mol. Sci. 24 (2023) 9191, https://doi.org/10.3390/ijms24119191.
[78] L. Yang, S. Pierce, T.W. Gould, G.L. Craviso, N. Leblanc, Ultrashort nanosecond electric pulses activate a conductance in bovine adrenal chromaffin cells that involves cation entry through TRPC and NALCN channels, Arch. Biochem. Biophys. 723 (2022) 109252, https://doi.org/10.1016/j.abb.2022.109252.
[79] R.C. Burke, S.M. Bardet, L. Carr, S. Romanenko, D. Arnaud-Cormos, P. Leveque, R. P. O'Connor, Nanosecond pulsed electric fields depolarize transmembrane potential via voltage-gated K+, Ca2+ and TRPM8 channels in U87 glioblastoma cells, Biochimica et Biophysica Acta (BBA) -, Biomembranes 1859 (2017) 2040–2050, https://doi.org/10.1016/j.bbamem.2017.07.004.
[80] P.A. Garcia, B. Kos, J.H. Rossmeisl Jr., D. Pavliha, D. Miklavčič, R.V. Davalos, Predictive therapeutic planning for irreversible electroporation treatment of spontaneous malignant glioma, Med. Phys. 44 (2017) 4968–4980, https://doi.org/10.1002/mp.12401.
[81] E. Acerbo, S. Safieddine, P. Weber, B. Botzanowski, F. Missey, M. Carrère, R. E. Gross, F. Bartolomei, R. Carron, V. Jirsa, I. Vanzetta, A. Trébuchon, A. Williamson, Non-thermal electroporation ablation of epileptogenic zones stops seizures in mice while providing reduced vascular damage and accelerated tissue recovery, Front. Behav. Neurosci. 15 (2021) 774999, https://doi.org/10.3389/fnbeh.2021.774999.
[82] C.J. Bradley, D.E. Haines, Pulsed field ablation for pulmonary vein isolation in the treatment of atrial fibrillation, J. Cardiovasc. Electrophysiol. 31 (2020) 2136–2147, https://doi.org/10.1111/jce.14414.
[83] V.Y. Reddy, S.R. Dukkipati, P. Neuzil, A. Anic, J. Petru, M. Funasako, H. Cochet, K. Minami, T. Breskovic, I. Sikiric, L. Sediva, M. Chovanec, J. Koruth, P. Jais, Pulsed field ablation of paroxysmal atrial fibrillation. 1-year outcomes of IMPULSE, PEFCAT, and PEFCAT II, JACC: Clinical Electrophysiology. 7 (2021) 614–627, https://doi.org/10.1016/j.jacep.2021.02.014.
[84] B. Geboers, H.J. Scheffer, P.M. Graybill, A.H. Ruarus, S. Nieuwenhuizen, R.S. Puijk, P.M. van den Tol, R.V. Davalos, B. Rubinsky, T.D. de Gruijl, D. Miklavčič, M. R. Meijerink, High-voltage electrical pulses in oncology: irreversible electroporation, electrochemotherapy, gene electrotransfer, electrofusion, and electroimmunotherapy, Radiology 295 (2020) 254–272, https://doi.org/10.1148/radiol.2020192190.